Prostate Boundary Detection in Transrectal Ultrasound Images

Ying Zhang [1], Wei Qian [2] and Ravi Sankar [1]
[1] Department of Electrical Engineering, University of South Florida, Tampa, FL
[2] H.Lee Moffitt Cancer Center & Research Institute, Tampa, FL

ABSTRACT

The objective of this paper is to improve prostate boundary detection system by modifying a set of preprocessing algorithms including tree-structured nonlinear filter (*TSF*), directional wavelet transforms (*DWT*) and tree-structured wavelet transform (*TSWT*). A new advanced automatic edge delineation model for the detection and diagnosis of prostate cancer on transrectal ultrasound (TRUS) images is presented. The model consists of a preprocessing module and a segmentation module. The preprocessing module is implemented for noise suppression, image smoothing and boundary enhancement. The active contours model is used in the segmentation module for prostate boundary detection in two-dimensional (2D) TRUS images. Experimental results show that the preprocessing module improves the accuracy and sensitivity of the segmentation module greatly when a comparison made on the segmented images between those with preprocessing and those without preprocessing. It is believed that the proposed automatic boundary detection module for the TRUS images is a promising approach, which provides an efficient and robust detection and diagnosis strategy and acts as "second opinion" for the physician's interpretation of prostate cancer.

1. INTRODUCTION

Prostate cancer is one of the most common types of cancer found in American men. It is estimated that there will be about 230,900 new cases of prostate cancer in the United States in 2004. (American Cancer Society, http://www.cancer.org). It is no doubt that early detection of cancer will improve the survival rate tremendously. Transrectal ultrasound (TRUS) scanning of the prostate is commonly utilized as the routine manner of prostate cancer detection and diagnosis [1]. Boundaries and volumes obtained from TRUS images play a key role in clinical decisions, since accurate boundary delineation is essential to guarantee preservation of organ function while controlling organ-confined cancer [2].

TRUS imaging has experienced several engineering advancements over the past 30 years, which has resulted in improved qualitative visual inspection of the image in real-time by a trained physician [3]. In spite of recent advances in ultrasonic imaging, manual boundary delineation on TRUS images by physicians is still a challenging task due to poor contrast between the prostate and its surrounding tissues; missing boundary segments; low SNR, speckle noise and refraction artifacts of the images. Besides, it is tedious and sensitive to observer bias and experience. It is demonstrated that visual interpretation of gray scale images is not highly accurate in identifying the internal architectural changes [4]. This limitation is partially due to the fact that human eye is capable of distinguishing only about 30 gray tones between black and white [3]. Thus, automated boundary delineation that can remove the physical weaknesses and subjectivity of observer interpretation within ultrasound images is essential for the early detection and treatment of prostate cancer.

Research has been initiated into automatic algorithms with minimal manual involvement that could segment the prostate boundaries from TRUS images accurately and effectively. In this paper, the proposed segmentation algorithm is implemented in 2D TRUS images. The segmentation algorithm includes two modules: the preprocessing module and the segmentation module. Due to the inherent noise in TRUS image, the preprocessing module including tree-structured nonlinear filter (TSF), directional wavelet transform (DWT) and tree-structured wavelet transform (TSWT) is implemented to improve the image by reducing noise and enhancing the resolution. In the segmentation module, active contour model is used for prostate boundary delineation. It has been proven that active contour model is more advantageous than other edge detectors by considering 2D spatial information [5].

The preprocessing module presented in this study is vital to the resulting segmented image. It reduces false edges and makes the prostate boundary detection efficiently. A comparison between the segmented image with preprocessed and the one without preprocessed shows that the preprocessing module has a great improvement on the accuracy of boundary detection.

The organization of this paper is as follows: Section 2 presents the 2D segmentation method. The evaluation results are described in Section 3 followed by the conclusion and plans for future study.

2. TWO-DIMENSIONAL COMPUTER-AIDED DIAGNOSIS ALGORITHMS

Shao et al. [6] classified the algorithms for prostate boundary delineation in 2D TRUS images into three categories: edge-based methods, texture-based methods and model-based methods.

Most recent research has shown that model-based segmentation methods are more efficient and powerful in delineating object boundaries [6]. Some prior knowledge, such as anatomic information, physical characteristics of the object and radiological features of imaging [7], is integrated to this algorithm. Methods based on deformable contour models are physically motivated, model-based techniques for delineating object boundaries by using closed curves or surfaces that deform under the influence of internal and external forces [7].

For accurately delineating prostate boundaries, in this paper, 2D TRUS images are processed for noise reducing and artifact removing before the deformable contour model is implemented in the segmentation module. Figure 1 shows the flowchart of this procedure.

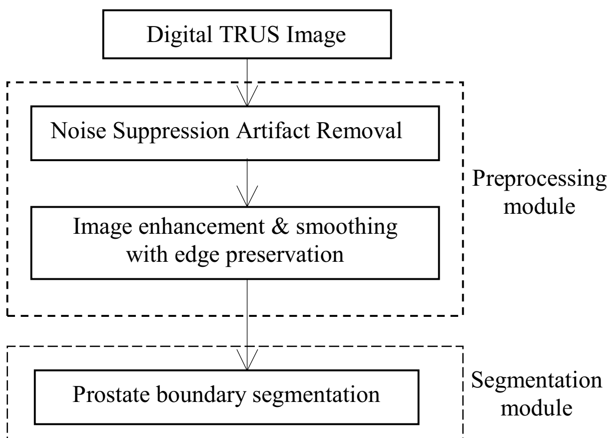

Figure 1. Flowchart of the Prostate Delineation Algorithm

2.1 Preprocessing Module

The preprocessing module, which has been used and tested successfully in mammography, plays a key role for the accurate boundary delineation of TRUS images because of the noisy characteristics and bad contrast of ultrasound images. It suppresses noise and artifacts, enhances edge information in the TRUS images, and makes the follow-up segmentation module works efficiently. The preprocessing module is composed of three algorithms: tree-structured nonlinear filtering (TSF), directional wavelet transforms (DWT) and tree-structured wavelet transforms (TSWT).

The major advantages of *TSF* for noise suppression and artifact removal are that its implementation does not require *a prior knowledge* of the local statistics within the filter window and its computational efficiency [8]. As a symmetric multistage filter, *TSF* combines the advantages of central weighted median filters (CWMF), linear and curved windows, and multistage operations that sequentially compare filtered and raw image data with the objective of obtaining more robust characteristics for noise suppression and detail preservation [8]. CWMF is a non-linear image smoothing and enhancement technique. It is especially effective at reducing both signal dependent and random noise [8]. To improve the performance of the CWMF, the use of a square window size of $N \times N$ pixels with different linear and curved shapes and the use of a series of CWMF in multistage tree-structured architecture are modified for the filter. Therefore, the CWMF is modified to be a 5×5 window with $2N$-2 linear or curved "sticks". A three-stage architecture is empirically selected in this study which combined good balanced performance, ease of implementation, and fast processing times.

Wavelet models can be described as multi-channel frequency decomposition filters that contain both frequency and directional information as opposed to the Fourier transform, which contains only frequency information. The directional wavelet transform (DWT) is a wavelet transform for multi-orientation signal decomposition. Implemented on a pixel-by-pixel basis, *DWT* allows enhancement of structures that have a specific orientation in the image. Two output images are obtained from the feature decomposition with directional wavelet analysis [9]. One is a directional texture image. It could be used for directional feature enhancement. The other is the smoothed version of the original image with directional information removed.

The M-channel *TSWT* is a highly efficient multi-resolution representation method for image enhancement. It has the advantage that can be readily expanded to $M \times M$ different resolution information to generate M^2 subimages [10]. *TSWT* is designed to zoom into desired frequency channels and perform selective decomposition and reconstruction of ROI in TRUS image. The lower resolution characteristics are useful for localization of the suspicious areas, while the information in the high resolution is essential for fine detail in segmentation module.

2.2 Segmentation Module

The *snake* used in this module is for prostate edge outlining in TRUS images. *Snakes*, first proposed by Kass et al. in 1980's, is a specific example of deformable model [11]. It is an energy-minimizing spline and controlled by minimizing a function which converts high-level contour information like curvature and discontinuities and low-level image information like edge gradients and terminations into energies. From a given starting point, it deforms itself to conform to the nearest salient contour.

The snake algorithm requires a set of initial contours as an input to the energy minimization process [12]. The anatomical prostate contour is an optimal choice as the initial contour because it is reasonable, less subjective and less variation. Figure 2 (c) shows the initial contour laid on the TRUS image for boundary segmentation.

The snake is an open or closed contour represented parametrically as $v(s) = (x(s), y(s))$, where $x(s)$ and $y(s)$ are the coordinates along the contour and $s \in [0,1]$. It defines desired image boundaries in an autonomous fashion by using the internal and image energy forces. The total energy along the contour is:

$$E_{snake} = \int_0^1 [E_{\text{int}}(v(s)) + E_{image}(v(s))]ds \qquad (2.1)$$

where E_{int} is the internal energy of the spline due to bending; E_{image} is the image force. The internal forces enforce the smoothness. It emanate from the shape of the snake. The image force attracts the contour to the desired features.

The internal energy of the contour depends on the shape of the contour and can be written:

$$E_{\text{int}} = \alpha(s)\left|\frac{dv}{ds}\right|^2 + \beta(s)\left|\frac{d^2v}{ds^2}\right| \qquad (2.2)$$

where the constant $\alpha(s)$ controls the tension along the spine; $\beta(s)$ controls the rigidity of the spine. The first derivative term $|v'(s)|^2$ discourages stretching and makes the model behave like an elastic string or membrane. The second derivative term $|v''(s)|^2$ discourages bending and makes the model behave like a rigid rod or thin plate.

The image force is a weighted combination of different functions. It can be expressed as:

$$E_{image} = E_{line} + E_{edge} \qquad (2.3)$$

The line-based functional E_{line} may be very simple:

$$E_{line} = f(x, y) \qquad (2.4)$$

where $f(x, y)$ denotes image gray levels at image location (x, y).

The edge-based functional E_{edge} attracts the snake to contours with large image gradients, which is to locations of strong edges:

$$E_{edge} = -|\nabla f(x, y)|^2 \qquad (2.5)$$

$\nabla f(x, y)$ calculates the gradient of the enhanced image from the preprocessing module.

In accordance with the calculus of variations, the final contour that minimizes the total energy is found by solving the vector valued partial differential (Euler-Lagrange) equation [13]:

$$\frac{\partial E_{snake}}{\partial v} = -\frac{\partial v}{\partial s} = \frac{\partial}{\partial s}\left(\alpha\frac{\partial v}{\partial s}\right) + \frac{\partial^2}{\partial s^2}\left(\beta\frac{\partial^2 v}{\partial s^2}\right) + \nabla f(v) = 0 \qquad (2.6)$$

This equation can be minimized by using the gradient-descent method to obtain the final contour. Having discretization on the contour and covert it to a vector v simplifies Equation (2.6). Let $v(s)$ be $v_i(s)$, $(i = 1, 2, \ldots, N)$, then

$$\frac{\partial v(s)}{\partial s} \rightarrow v_{i+1}(s) - v_i(s) \qquad (2.7)$$

The final solution is:

$$v_{j+\Delta j} = M^{-1}\left(v_j + \nabla F(v_j)\cdot\Delta j\right) \qquad (2.8)$$

where M is a pentadiagonal matrix, whose diagonal element is the sequence of β, $-\alpha-4\beta$, $1+2\alpha+6\beta$, $-\alpha-4\beta$, β.

Figure 2 shows the results of the segmentation algorithm in 2D TRUS images.

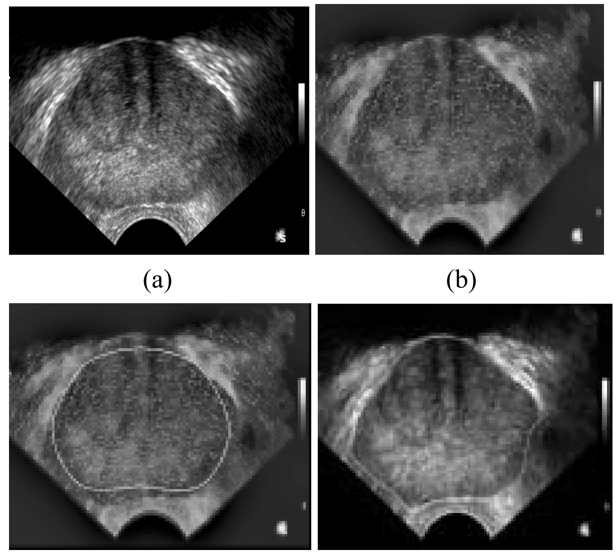

(a) (b) (c) (d)

Figure 2. Segmentation Results on 2D TRUS Images (a)Original Image (b) Corresponding Output Image after Preprocessing (c) Preprocessed Image with the Initial Contour Laid on (d) the Final Contour Image with the Prostate Boundaries Segmented at α=0.3 and β= 0.5

3. EVALUATION AND RESULTS

Seven sets of data are included to test the accuracy of the algorithm. Each set of data has 7 to 8 images which are collected in parallel planes. The spatial distance between these planes is 5 *mm* in our case. Therefore, a total of 51 images are used in the verification of the algorithm.

The computer-defined boundary on each TURS image is compared with the truth file by area-based metrics. Area-based metrics are insensitive to shape and calculated using the different areas defined by the computer and by manual [12]. Three area-based metrics can be defined.

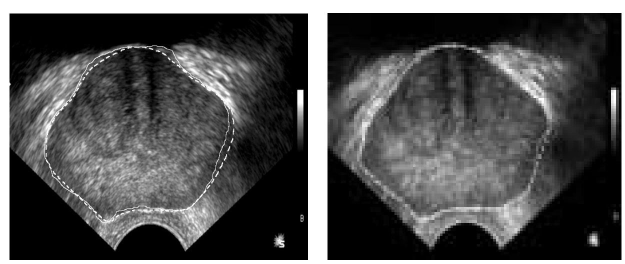

(a) (b)

Figure 3. Manual Outlined Structures are Overlaid on the Automatic Boundary Segmentation Images. *Dotted line*: manually outlined boundary. *Solid line*: computer-defined boundary. (a) Without the preprocessing module implementation on TRUS images (b) The preprocessing module is implemented on TRUS images before the segmentation module is processed.

In Figure 3, the TRUS segmentation images with manual outlined and computer-aided outlined are presented.

It is obvious that preprocessing module removing image noise, smoothing images and enhancing the image resolutions can improve the performance of the segmentation module significantly. Figure 3 (a) shows the comparison between manually outlined boundary and computer-aided outlined boundary without implementing the preprocessing module. Figure 3 (b) shows the comparison after the preprocessing module is implemented.

The evaluation results calculated by the area-based metrics are shown in Table 1.

Area-Based Metrics	Percentage (%) **(WITHOUT** Preprocessing)	Percentage (%) **(WITH** Preprocessing)
Fractional Area Difference	2.3	1.2
Sensitivity	92.7	98.2
Accuracy	91.3	97.4

Table 1. Evaluation results of the segmented images based on area-based metrics

It can be observed from the results that the preprocessing module reduces the difference between the boundaries defined by the truth file and the boundaries delineated by computer. The sensitivity and the accuracy of the segmentation module have been improved too.

The distances between the computer estimates of the prostate boundaries and the manual outlining on the same image are given in Table 2.

51 Images	Mean Absolute Distance (*MAD*)	
	Mean	Standard Derivation
Manual delineation	1.79 (mm)	1.51 (mm)
Computer-aided segmentation	1.28 (mm)	0.56 (mm)

Table 2. The mean distances between CAD detection and their corresponding truth files.

4. CONCLUSION AND FUTURE WORK

Semi- or automatic prostate boundary detection methods provide robust, consistent and reproducible results with a certain degree of accuracy. It is unlikely that automatic prostate boundary detection methods will ever replace physicians [6]. However, as the “second opinion” for the physicians during the routine clinical setting, computer-aided segmentation techniques have been widely used in the detection and diagnosis of breast cancer, lung cancer and prostate cancer.

In this study, the preprocessing module which includes *TSF*, *DWT* and *TSWT* for noise suppression and image enhancement is implemented. The resulting images are further processed by the segmentation module for boundary delineation. It improves sensitivity and accuracy of the segmentation significantly. In the segmentation module, the *snake* algorithm is modified and implemented on the 2D TRUS images. The evaluation results for this segmentation algorithm show that it is an efficient boundary delineation method among the edge segmentation algorithms.

In order to provide more accurate and direct view of the prostate structure during the clinical examination for physicians, 3D reconstruction of the prostate can be proposed based on the algorithms implemented on 2D images in the future. The data collection in 3D space is in the form of a sequence of 2D image planes. The preprocessing module presented in this study can be implemented on each 2D TRUS images before the 3D rendering. It will help to reduce false edges in a great amount during the segmentation process. Therefore, it is efficient for the 3D segmentation algorithm implementation. It is obvious that this combination of both 2D and 3D information of prostate will significantly enhance the physicians' situation awareness and thus lead to a substantial improved performance of cancer detection.

References

[1] E. Feleppa et al., Typing of Prostate Tissue by Ultrasonic Spectrum Ananlysis", IEEE Transactions on Ultrasonics, Ferroelectrics and Frequency Control: 43: 4, 609-619, 1996

[2] J. Priestly et al., Guided Brachytherapy for the Treatment of Confined Prostate Cancer, Urology: 40, 27-32, 1992

[3] A. Houston et al., Prostate Ultrasound Image Analysis: Localization of Cancer Lesions to Assist Biopsy, CBMS'95, Lubbock, Texas, 1995

[4] R. Huben, The USA Experience: Diagnosis and Follow-up of Prostate Malignancy by Transrectal Ultrasound, Progress in Clinical and Biological Research, 237:153-159, 1987

[5] R. Chang et al., 3D Snake for US in Margin Evaluation for Malignant Breast Tumor Excision Using Mammotome, IEEE Transactions on Information Technology in Biomedicine:7:3, 197-201, 2003

[6] F. Shao et al., Prostate Boundary Detection from Ultrasonographic Images, Ultrasound Med. 605-623, 2003

[7] Y. Zhan et al., Automated Segmentation of 3D US Prostate Images Using Statistical Texture-Based Matching Method, MICCAI 2003, LNCS 2878, 688-696, 2003

[8] W. Qian et al., Tree-Structured Nonlinear Filters in Digital Mammography, IEEE Transactions on Medical Imaging: 13: 1, 25-36, 1994

[9] L. Li et al., Digital Mammography: Computer-Assisted Diagnosis Method for Mass Detection with Multiorientation and Multiresolution Wavelet Transforms, Acad Radiol: 4, 724-731, 1997

[10] W. Qian et al., Tree-Structured Wavelet Transform Segmentation of Microcalcifications in Digital Mammography, Med. Phys.: 22, 1247-1254, 1995

[11] M. Kass et al., Snakes: Active contour models, International Journal of Computer Vision, 1:321–331, 1988

[12] H. Ladak et al., Prostate Boundary Segmentation from 2D Ultrasound Images, Med. Phys.:27, 1777-1788, 2000

[13] G. Yang et al., Edge Based Segmentation & Active Contours, Computer Vision: 1-5